Numerical modeling of large field-induced strains in ferroelastic bodies: a continuum approach

2008 J. Phys.: Condens. Matter 20 204126

(http://iopscience.iop.org/0953-8984/20/20/204126)

J. Phys.: Condens. Matter **20** (2008) 204126 (5pp) doi:10.1088/0953-8984/20/20/204126

Numerical modeling of large field-induced strains in ferroelastic bodies: a continuum approach

Yu L Raikher and O V Stolbov

Institute of Continuous Media Mechanics, Ural Branch of the Russian Academy of Sciences, 1 Korolyov street, Perm, 614013, Russia

E-mail: raikher@icmm.ru

Received 1 April 2008
Published 1 May 2008
Online at stacks.iop.org/JPhysCM/20/204126

Abstract

A consistent continuum model of a soft magnetic elastomer (SME) is presented and developed for the case of finite strain. The numeric algorithm enabling one to find the field-induced shape changes of an SME body is described. The reliability of the method is illustrated by several examples revealing specifics of the magnetostriction effect in SME samples of various geometries.

1. Introduction

Soft magnetic elastomers (SMEs) are known under many names: magnetorheological [1] and magnetoactive [2] polymers, elastomagnets [3], magnetoelastics [4, 5], ferrogels [6] etc; in some works no special name is ascribed [7, 8]. This variety is due on the one hand to numerous interesting properties of SMEs, and on the other to a plethora of applications they are considered to be unique for. With regard to their structure, SMEs are composite magnetically controlled functional materials based on weakly linked highly elastic matrices filled with magnetic particles of micron or submicron size. One of the most remarkable features of these media is a giant magnetic-strain (striction) effect [4, 6] which appeals for practical use. Indeed, magnetic strains in SMEs exceed any classical magnetostriction by many orders of magnitude and range to tens and hundreds per cent. This is not a surprise, however, since the strain-inducing mechanism has nothing in common with crystallophysics. In SMEs, application of a field induces ponderomotive forces acting on Ampere currents circulating in magnetized particles; via the particles, these forces are exerted on the matrix. The resulting magnetic stress deforms the body along the direction of the field or stretches it towards the region where the field is maximal. The equilibrium is reached when this tendency is balanced by the elastic stress striving to preserve the initial shape of the sample.

For an SME, due to its softness, shape change (deformation) makes an effective way to reduce the free energy. Let us estimate the range of elastic moduli within which the magnetic strain produced by a moderate field becomes appreciable. We take the field to be about 1 kOe and the spatial scale of non-uniformity $\sim$1 cm; these conditions are achievable in any laboratory. In a uniform field, modeling a sample with an ellipsoid, we write the magnetic energy gain as $M^2\Delta\mathcal{N}$, where $\Delta\mathcal{N}$ is the change in the demagnetizing factor due to deformation, and M is the SME magnetization. Equally simple, the increment of the elastic energy is $\sim E\varepsilon^2$, where E is the Young modulus and ε is the strain. Comparison yields $E \sim M^2\Delta\mathcal{N}/\varepsilon^2$. For $M \sim 100$ G and $\Delta\mathcal{N} \sim \varepsilon \sim 0.1$, i.e. a 10% strain, one finds the elastic modulus $E \sim 10$ kPa, that is two to four orders of magnitude lower than in rubbers. In a non-uniform field the strain is induced by bulk magnetic forces. Setting their work spent on dragging a material element by distance 1 cm equal to the elastic energy increment at 100% strain, one gets for the modulus the same reference value, $E \sim 10$ kPa. Naturally, the deforming action of a non-uniform field is much higher than that of a uniform one. In general, these estimates justify the viewpoint of SMEs as a special class of magnetically sensitive media different from usual magnetic elastomers (rubbers) [10]. Real SME are made on the base of weakly linked silicone caoutchoucs [4, 5], polyvinyl alcohol and polyacrylamide [6] or polystyrene [11] polymeric gels, etc.

To date there has been no exhaustive theory describing magnetic strain in SMEs, although some serious attempts on this should be noted [12–14]. In what follows we present an account of a model that is both the most simple and the most advanced one. Namely, we consider a continuum approximation that treats the SME as a homogeneous elastic

isotropically magnetizable substance. The goal of this short review is to show that despite its obvious shortcomings the model is practical and capable of providing reasonable results in agreement with experiment.

2. Magnetoelasticity equations at finite strains

A study of strain induced by a uniform field is both more simple and more appropriate for working out an adequate magnetomechanics of SMEs. Once built up, such a theory may be easily modified for non-uniform fields. Besides this, a simplified magnetic part allows us to focus on the solution algorithm. The point is that the magnetic energy gain is important only if the shape change of the sample is considerable. As this gain is determined by internal field H, which, in turn, depends on the sample shape, an essentially coupled magnetoelastic problem arises that is to be solved in a spatial region of which the boundary is also a sought for issue.

Aiming at the problems with allowance for finite strain, i.e. large shape changes, it is convenient to introduce two configurations: initial (non-deformed) and actual (deformed) [15]. The radius-vector of a point in the initial state is $\boldsymbol{r}$, in the actual one it is $\boldsymbol{R} = \boldsymbol{r} + \boldsymbol{u}$, where $\boldsymbol{u}$ is displacement vector. Then the basis vectors of the initial state are $\boldsymbol{\epsilon}_i = \partial \boldsymbol{r}/\partial q_i$ and those of the actual one $\hat{\boldsymbol{\epsilon}}_i = \partial \boldsymbol{R}/\partial q_i$, where q_i are reference Lagrange coordinates. Hamilton operators are defined as $\nabla = \boldsymbol{\epsilon}^i \partial/\partial q_i$ and $\hat{\nabla} = \hat{\boldsymbol{\epsilon}}^i \partial/\partial q_i$, respectively. A basic kinematic quantity, the deformation gradient, in a system with metric tensor $\mathbf{g}$ is

$$\begin{aligned} \mathbf{F} &= (\nabla \boldsymbol{R})^{\mathrm{T}} = \hat{\boldsymbol{\epsilon}}_i \boldsymbol{\epsilon}^i = \mathbf{g} + (\nabla \boldsymbol{u})^{\mathrm{T}}, \\ \mathbf{F}^{-1} &= (\hat{\nabla} \boldsymbol{r})^{\mathrm{T}} = \boldsymbol{\epsilon}_i \hat{\boldsymbol{\epsilon}}^i = \mathbf{g} - (\hat{\nabla} \boldsymbol{u})^{\mathrm{T}}, \end{aligned} \tag{1}$$

where lower/upper indices denote covariant/contravariant components, respectively.

A complete set of equations for the equilibrium magnetodeformational effect unites two problems: magnetostatic and elastic. We start with the magnetic part. In the absence of electric currents, the magnetic field strength $\boldsymbol{H}$ is presented in terms of magnetic potential as $\boldsymbol{H} = \boldsymbol{H}_0 - \hat{\nabla}\psi$, where $\boldsymbol{H}_0$ is the external field. By definition, magnetic induction and magnetization are related to each other by $\boldsymbol{B} = \boldsymbol{H} + 4\pi \boldsymbol{M}$. From the solenoidality condition $\hat{\nabla} \cdot \boldsymbol{B} = 0$ follows the Poisson equation

$$\hat{\nabla}^2 \psi = 4\pi \hat{\nabla} \cdot \boldsymbol{M}. \tag{2}$$

In the general case, the magnetization at a given point depends on both the local field strength and mechanical strain. Therefore, we assume the equation of magnetic state in the form $\boldsymbol{M} = \boldsymbol{M}(\boldsymbol{H}, \mathbf{C})$, where $\mathbf{C} = \mathbf{F}^{\mathrm{T}} \cdot \mathbf{F}$ is the right Cauchy–Green deformation tensor. Equation (2) is solved with the usual magnetostatic boundary conditions at the sample surface Γ:

$$\begin{aligned} \left(\partial \psi^{(\mathrm{i})}/\partial N\right)_\Gamma - \left(\partial \psi^{(\mathrm{e})}/\partial N\right)_\Gamma &= 4\pi \boldsymbol{M} \cdot \boldsymbol{N}|_\Gamma, \\ \psi^{(\mathrm{i})}|_\Gamma &= \psi^{(\mathrm{e})}|_\Gamma, \end{aligned} \tag{3}$$

where indices (i) and (e) denote the inner and outer spaces and $\boldsymbol{N}$ is the outer normal.

The force balance equation that determines the equilibrium state of the sample is

$$\hat{\nabla} \cdot \mathbf{T} + (\boldsymbol{M} \cdot \hat{\nabla}) \boldsymbol{H} = 0, \tag{4}$$

where $\mathbf{T}$ is the Cauchy stress tensor. At the surface of the sample the condition $\boldsymbol{N} \cdot \mathbf{T}|_\Gamma = 2\pi M_N^2 \boldsymbol{N}|_\Gamma$ holds, with $M_N = \boldsymbol{M} \cdot \boldsymbol{N}$ being the normal component of magnetization.

In general, the elastic potential of an SME that is isotropic at $\boldsymbol{H}_0 = 0$ is written as [13, 14]

$$W = W\left(I_1(\mathbf{C}), I_2(\mathbf{C}), I_3(\mathbf{C}), M^2\right), \tag{5}$$

where I_j are principal tensor invariants. As soon as the elastic potential is defined, one obtains the Cauchy stress tensor in the form [15]

$$\mathbf{T} = 2J^{-1} \mathbf{F} \cdot (\partial W/\partial \mathbf{C}) \cdot \mathbf{F}^{\mathrm{T}}, \tag{6}$$

with $J = I_3(\mathbf{F})$ being a Jacobian; for an incompressible medium $J = 1$.

In the framework of our model the free energy density of SME is written as

$$\mathcal{F} = -\int_0^H \overset{\circ}{M}(H)\, \mathrm{d}H + \overset{\circ}{W} + \alpha \overset{\circ}{M}{}^2(H)\, [I_1(\mathbf{C}) - 3], \tag{7}$$

where $\overset{\circ}{W}$ is the elastic potential at $H_0 = 0$ and $\overset{\circ}{M}(H)$ the magnetization law at zero strain; α is a parameter that characterizes the coupling of local magnetization and strain. For $\overset{\circ}{W}$, assuming an incompressible SME, we take the Mooney–Rivlin potential

$$\overset{\circ}{W} = C_1[I_1(\mathbf{C}) - 3] + C_2[I_2(\mathbf{C}) - 3]. \tag{8}$$

From equations (6)–(8) the stress in terms of the left Cauchy–Green deformation tensor $\mathbf{B} = \mathbf{F} \cdot \mathbf{F}^{\mathrm{T}}$ is written

$$\begin{aligned} \mathbf{T} = -p\,\mathbf{g} + 2\left[C_1(1 + \alpha \overset{\circ}{M}{}^2) + C_2 I_1(\mathbf{C})\right] \mathbf{B} - 2C_2 \mathbf{B} \cdot \mathbf{B}, \\ I_3(\mathbf{B}) = 1; \end{aligned} \tag{9}$$

for an incompressible material the net pressure p emerges as an independent variable.

The magnetic equation of state is given by

$$\boldsymbol{M} = -\frac{\partial \mathcal{F}}{\partial \boldsymbol{H}} = \left\{ \overset{\circ}{M} - 2\alpha \overset{\circ}{M} \frac{\partial \overset{\circ}{M}}{\partial H} \left[I_1(\mathbf{C}) - 3\right] \right\} \frac{\boldsymbol{H}}{H}. \tag{10}$$

We concede two variants of the 'unperturbed' magnetization law: a linear one $\overset{\circ}{\boldsymbol{M}} = \chi \boldsymbol{H}$ and one modeling saturation $\overset{\circ}{\boldsymbol{M}} = M_0 L(\gamma H)\, \boldsymbol{H}/H$, where χ is the susceptibility, M_0 the saturation magnetization of the SME and γ a parameter of the Langevin function L.

For an SME sample characterized by energy (7), the force and field balance relations (2) and (4) with the aid of Maxwell equations and pertinent boundary conditions may be re-written in the form of two variational equations:

$$\begin{aligned} \int_{V^{(i)}} \delta W\, \mathrm{d}V &= \int_\Gamma \left[2\pi M_N^2 \boldsymbol{N} + \boldsymbol{N} \cdot \mathbf{S}\right] \cdot \delta \boldsymbol{u}\, \mathrm{d}S \\ &\quad - \int_{V^{(i)}} \mathbf{S} \cdot\cdot \hat{\nabla} \delta \boldsymbol{u}\, \mathrm{d}V, \\ \int_{V^{(i)}+V^{(e)}} \hat{\nabla}\psi \cdot \hat{\nabla} \delta\psi \mathrm{d}V &= 4\pi \int_{V^{(i)}} \boldsymbol{M} \cdot \hat{\nabla} \delta\psi \mathrm{d}V, \end{aligned} \tag{11}$$

where $\mathbf{S} = (1/4\pi)(\boldsymbol{H}\boldsymbol{B} - \frac{1}{2}\mathbf{g}H^2)$ is the Maxwell stress tensor, and W the elastic potential with allowance for magnetic terms; W differs from $\mathring{W}$ of equation (8) solely by a renormalized first constant: instead of C_1 it contains $(C_1 + \alpha M^2)$.

Equations (7)–(11) make a full set to evaluate the equilibrium shape of an SME sample and corresponding distributions of the magnetic field, magnetization and internal mechanical stress at finite increments of all the latter variables. By this the main drawback of the former continuum SME models, the small, i.e. infinitesimal, strain limit, is overcome. Apparently, for the systems with large shape changes, the small-strain limit, although convenient for preliminary analysis, is hardly more than a 'poor man's tool'.

3. Algorithm

The problem of field-induced deformation of an SME sample is nonlinear both physically and geometrically. The fact that the sample boundary is not fixed but is itself the subject of evaluation rules out the majority of conventional numeric tools based on the finite-element method (FEM). From our experience, an efficient way out, at least for two-dimensional problems, is provided by the open-code FreeFEM++ package [16].

In our scheme a nonlinear magnetoelastic problem is solved as a sequence of linear ones. Its elastic part is given by a linearized form of the first of integral equations (11):

$$\int_{V^{(i)}} \left[\mathbf{T}_1 \cdot\cdot\, \delta\hat{\mathbf{e}} + I_1(\hat{\mathbf{e}})\delta p\right] \mathrm{d}V = -\int_{V^{(i)}} \left\{(\mathbf{T}' - \mathbf{T}'_1) \cdot\cdot\, \delta\hat{\mathbf{e}} + \left[I_3(\mathbf{F}') - I_1(\hat{\mathbf{e}}') - 1\right]\delta p\right\} \mathrm{d}V + \int_{\Gamma} \left[2\pi M_N^2 \boldsymbol{N} + \boldsymbol{N}\cdot\mathbf{S}\right]\cdot\delta\boldsymbol{u}\,\mathrm{d}S - \int_{V^{(i)}} \mathbf{S}\cdot\cdot\,\hat{\nabla}\delta\boldsymbol{u}\,\mathrm{d}V, \tag{12}$$

where $\hat{\mathbf{e}} = \frac{1}{2}(\hat{\nabla}\boldsymbol{u} + \hat{\nabla}\boldsymbol{u}^{\mathrm{T}})$ and $\mathbf{T}_1 = -p\,\mathbf{g} + 4C_1\hat{\mathbf{e}}$ is the part of the stress tensor $\mathbf{T}$ that is linear in displacements. In equation (12) the prime denotes the solutions at the preceding step.

The linearized magnetostatic problem is written

$$\int_{V^{(i)}} \hat{\nabla}\psi\cdot\delta\psi\,\mathrm{d}V + 4\pi\int_{V^{(i)}} \tilde{\chi}(H')\left[\hat{\nabla}\psi - \boldsymbol{H}_0\right]\cdot\hat{\nabla}\delta\psi\,\mathrm{d}V + \int_{V^{(e)}} \hat{\nabla}\psi\cdot\hat{\nabla}\delta\psi\,\mathrm{d}V = 0, \tag{13}$$

where $\tilde{\chi}(H) = M(H)/H$; for linear magnetization $\tilde{\chi} = \chi$. To the boundary conditions (3) imposed at the surface of a sample, a requirement is added that far from the body the magnetic potential coincides with that of a magnetic dipole of the moment $\boldsymbol{\mu} = \int_{V^{(i)}} \boldsymbol{M}\,\mathrm{d}V = \int_{V^{(i)}} \tilde{\chi}(H')\boldsymbol{H}\,\mathrm{d}V$.

A self-consistent algorithm that couples the solutions of the elastic (12) and magnetic (13) problems is organized as follows. First, a certain initial mesh is generated covering both the SME sample and a sufficient part of the space around it so that $V^{(e)} \gg V^{(i)}$. Then on this mesh the magnetostatic problem is solved in both inner and outer spaces; i.e., the instant shape of the body is fixed. As a result, the distributions of magnetic field and magnetic forces are found. Next, on the same mesh the elastic problem is solved with the surface and bulk forces determined from the solution of the magnetic problem. Thus, the strain distribution is found. Using it, the mesh is re-built and the process starts anew. The procedure is stopped when a penalty function that compares displacement fields at the iteration steps j and $j+1$ falls below a given level.

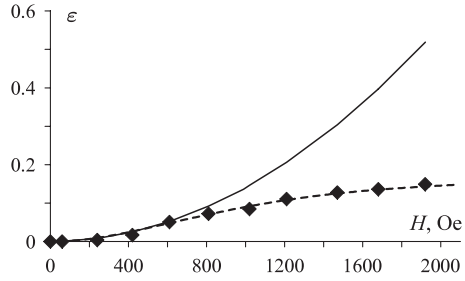

Figure 1. Magnetic striction of a cylinder, see the text for parameters.

4. Results and discussion

FreeFEM++ language is well developed only for 2D problems. With regard to this, we study the cases where an SME body is axisymmetrical and magnetized along its axis. Given this, a 3D problem might be solved with a 2D numeric tool.

4.1. Cylinder and prism

The case is instructive to show the advantages of the finite-strain approach. The experimental data (Stepanov, see acknowledgments) were obtained on a prism sample with dimensions $11 \times 4 \times 4$ mm^3 made of an iron carbonyl-based SME with the effective Young modulus $E = 16$ kPa (at zero field). The magnetization curve of the material is quasi-linear up to 1.5 kOe; the value of M achieved under $H_0 = 1$ kOe is about 200 G. The measurement results are plotted in figure 1 with filled dots.

Since the present theory could be applied in full only for axisymmetrical configurations, we replace the prism by an effective round cylinder whose length and end-wall area are equal to those of the prism. The external field $\boldsymbol{H}_0$ is uniform and directed along the cylinder axis. We note that except for an ellipsoid there is no analytical solution of the magnetostatic problem. So we obtain the net field and magnetization distributions numerically using FreeFEM++. Magnetization is assumed to obey a linear magnetic law with the susceptibility estimated from the measured magnetization curve. In the small-strain limit a single magnetic calculation is enough to evaluate the induced forces and the resulting strain field. To describe the magnetostriction effect, we define the elongation parameter as $\varepsilon = [l(H_0) - l(0)]/l(0)$, where $l(H_0)$ is the cylinder length along the field direction. The small-strain limit predicts universal scaling $\varepsilon \propto H_0^2/E$; the corresponding parabola is shown in figure 1 by a solid line. We note that

Figure 2. Formation of a 'dome' at an SME plate with $D/h = 10$ and $\chi = 0.2$ under the field $H = 1$ kOe; note the reconfiguration of the calculation mesh.

it does not contain any adjustable parameters since E and χ values are taken from independent tests.

As seen, at weak fields the small-strain curve is close to the measurement while at higher fields it progressively deviates from this. Remarkably, this deviation is quite large even in the interval $H_0 \lesssim 1.5$ kOe, where, according to the magnetic measurement, the linear magnetization law holds. To understand the cause of this divergence, the same problem is solved in a nonlinear statement by the numerical scheme described in section 3. Hereby the self-similarity of ε is no longer valid, and the obtained dependence $\varepsilon(H_0)$ pertains to the particular sample under study. Moreover, now the calculation incorporates an adjustable parameter α introduced in equation (7). The self-consistent numeric process converges well; the result of the calculation is plotted in figure 1 by a dashed line for $\alpha = 0.15$, which value is found by fitting. Comparison of the curves and data shows that for magnetostriction of a cylinder the finite-strain approach is able to provide good agreement with experiment in a wide range of fields.

4.2. Thin plate

Another example, being in general also a 'cylinder' problem, demonstrates completely different behavior. Consider a round thin plate of SME fixed over its rim and subjected to a uniform magnetic field normal to the plate surface. In the qualitative aspect, it is clear that for a thin plate to be positioned across $\boldsymbol{H}_0$ is most unfavorable with respect to the magnetic energy. To reduce it, the plate will strive to turn its plane along the field. As the rim is unmovable, this tendency is opposed by the elastic forces, which are strongest at the periphery of the plate. Accordingly, the center of the plate is the easiest-to-move point. Therefore, a possible response of the plate is to build up a round 'dome' where any radial line connecting the summit with the rim is now tilted to $\boldsymbol{H}_0$ at an angle smaller than $\pi/2$, thus contributing to the negative gain of the magnetic energy. In the problem studied, all the forces except for magnetic and elastic ones are neglected. Given this, the plate deflections in the directions parallel and antiparallel to $\boldsymbol{H}_0$ ('positive' and 'negative' domes), being spatially different, are energetically equivalent. This degeneration entails a fundamental consequence: with necessity the plane geometry of the plate may start to deform not earlier than the field strength H_0 reaches some finite (threshold) value. Therefore, the plate behavior is qualitatively different from the striction of a prolate cylinder. First, it breaks the inversion symmetry of the sample ($\pm\boldsymbol{H}_0$) and, second, it has a finite threshold. To be precise, we remark that for the plate a plain (zero-threshold) inversion-symmetrical striction described in the preceding subsection is also present, but is magnitude is negligible compared to the deflection mode.

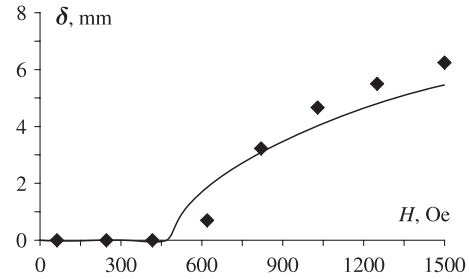

Figure 3. 'Dome' height for a plate with the parameters of figure 2; measured (points) and calculated (line).

The problem admits linear analysis, which for the threshold field yields

$$H_0^* \propto \sqrt{E}\,(4\pi + 1/\chi)\,h/R, \tag{14}$$

where h and R are the plate thickness and radius. The parametric dependences of the threshold rendered by equation (14) agree well with those predicted by the finite-strain calculation. Using the latter at $H_0 > H_0^*$, where the small-strain limit is inapplicable, one obtains the dome shapes of the SME plate; an example is given in figure 2. Comparison with experiment proves [17] the reliability of the model; see figure 3 for illustration.

4.3. Dumb-bell

Consider a dumb-bell consisting of two spheres of radii R whose centers are connected by a cylindrical rod of length $2h$ and radius r. This problem abuts closely on a single-sphere one. The magnetodeformational effect in isolated SME spheres and ellipsoids is studied in detail in [9]. These rounded objects stretch in the direction of the applied uniform field. In a dumb-bell, however, this tendency is opposed by mutual attraction of two magnetized bodies whose magnetic moments are parallel to the main axis. To consider the net elongation of the structure, two limiting cases could be foreseen with regard to the ratio r/R. Indeed, a dumb-bell with a thin neck ($r \ll R$) is mostly influenced by the sphere attraction. It overcomes the elastic resistance of the neck, and the net field-induced response is a contraction of the dumb-bell. In contrast, a dumb-bell with a neck $r \lesssim R$ is close to a prolate ellipsoid and as such elongates in the direction of $\boldsymbol{H}_0$. Therefore, for a given SME dumb-bell, just varying the geometry parameters, one can pre-determine the type of its behavior.

In the framework of the finite-strain algorithm, one is able to describe the striction of a dumb-bell with an arbitrary set of geometry and material parameters. In figure 4, as an example, the overall elongation ε defined similarly to that for a cylinder is shown as a function of the dumb-bell geometry. As seen, the qualitative predictions are confirmed in full: under a given field a dumb-bell could either stretch or contract while at the 'critical' value of r/R such a dumb-bell practically does not change its length.

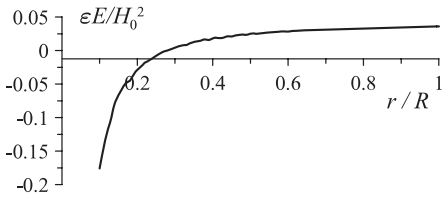

Figure 4. Magnetostriction of a dumb-bell with length $2h = 2.6R$; the magnetic susceptibility of the SME is $\chi = 0.2$.

5. Conclusions

A consistent model interpreting an SME as a magnetizable elastic continuum is presented. The set of equations describing the equilibrium shape of an SME body under finite deformation is given. An algorithm that employs the finite-element method is proposed, and the FreeFEM++ package is shown to be an appropriate calculation tool.

The approach developed is illustrated with three examples of SME bodies subjected to a uniform magnetic field. For a round cylinder the new description turns out to be essential for bringing together theory and experiment. For a thin plate a magnetomechanical instability is found and quantified. For an SME dumb-bell the theory predicts that the field-induced increment of its overall length is either positive or negative depending on the relation between the sphere and neck radii.

Acknowledgments

The authors acknowledge RFBR project 06-01-00723 and thank G V Stepanov for discussions and for providing experimental data prior to their publication.

References

[1] Ginder J M, Clark S M, Schlotter W F and Nichols M E 2002 *Int. J. Mod. Phys.* B **16** 2412
[2] Bellan B and Bossis G 2002 *Int. J. Mod. Phys.* B **16** 2447
[3] Lanotte L, Ausanio G, Hison C, Iannotti V, Luponio C and Luponio C Jr 2004 *J. Optoelectron. Adv. Mater.* **6** 523
[4] Nikitin L V, Mironova L S, Stepanov G V and Samus A N 2001 *J. Polym. Sci.* A **43** 443
[5] Nikitin L V, Mironova L S, Kornev K G and Stepanov G V 2004 *J. Polym. Sci.* A **46** 489
[6] Zrínyi M, Barsi L and Büki A 1996 *J. Chem. Phys.* **104** 8750
Zrínyi M, Barsi L and Büki A 1997 *Polym. Gels Networks* **5** 415
[7] Jolly M R, Carlson J D, Muñoz B C and Bullions T A 1996 *J. Intell. Mater. Syst. Struct.* **7** 613
[8] Carlson J D and Jolly M R 2000 *Mechatronics* **10** 555
[9] Raikher Yu L and Stolbov O V 2000 *Tech. Phys. Lett.* **26** 156
Raikher Yu L and Stolbov O V 2005 *J. Appl. Mech. Tech. Phys.* **46** 434
[10] Alekseev A G and Kornev A E 1987 *Magnetic Elastomers* (Moscow: Chemistry)
[11] Lattermann G and Krekhova M 2006 *Macromol. Rapid Commun.* **27** 1373
[12] Naletova V A, Turkov V A, Shkel Y and Klingenberg D 1999 *J. Magn. Magn. Mater.* **202** 570
[13] Borcea L and Bruno O 2001 *J. Mech. Phys. Solids* **49** 2877
[14] Kankanala S V and Triantafyllidis N 2004 *J. Mech. Phys. Solids* **52** 2869
[15] Lurye A 1980 *Nonlinear Elasticity Theory* (Moscow: Nauka)
[16] http://www.freefem.org
[17] Stepanov G V, Gorbunov A I, Raikher Yu L, Stolbov O V, Alekseeva E I, Levina E F and Kramarenko E Yu 2007 *Proc. 15th Winter School on Continuum Mechanics (Perm, Feb.–March 2007)* p 31